Fusion Engineering and Design 169 (2021) 112490

Contents lists available at ScienceDirect

Fusion Engineering and Design

journal homepage: www.elsevier.com/locate/fusengdes

Preliminary design of the COMPASS upgrade tokamak

P. Vondracek [a,*], R. Panek [a], M. Hron [a], J. Havlicek [a], V. Weinzettl [a], T. Todd [a], D. Tskhakaya [a], G. Cunningham [a], P. Hacek [a], J. Hromadka [a], P. Junek [a], J. Krbec [a], N. Patel [a], D. Sestak [a], J. Varju [a], J. Adamek [a], M. Balazsova [a], V. Balner [a], P. Barton [a,c], J. Bielecki [d], P. Bilkova [a], J. Błocki [d], D. Bocian [d], K. Bogar [a,c], O. Bogar [a], P. Boocz [a], I. Borodkina [a], A. Brooks [e], P. Bohm [a], J. Burant [a], A. Casolari [a], J. Cavalier [a], P. Chappuis [a], R. Dejarnac [a], M. Dimitrova [a], M. Dudak [a], I. Duran [a], R. Ellis [e], S. Entler [a], J. Fang [e], M. Farnik [a,b], O. Ficker [a,b], D. Fridrich [a], S. Fukova [a], J. Gerardin [a], I. Hanak [a], A. Havranek [a], A. Herrmann [f], J. Horacek [a], O. Hronova [a], M. Imrisek [a,c], N. Isernia [g], F. Jaulmes [a], M. Jerab [a], V. Kindl [i], M. Komm [a], K. Kovarik [a], M. Kral [a], L. Kripner [a,c], E. Macusova [a], T. Majer [a], T. Markovic [a,c], E. Matveeva [a,c], K. Mikszuta-Michalik [a,j], M. Mohelnik [a], I. Mysiura [a], D. Naydenkova [a], I. Nemec [a], R. Ortwein [d], K. Patocka [a], M. Peterka [a,c], A. Podolnik [a], F. Prochazka [a], J. Prevratil [a], J. Reboun [i], V. Scalera [g], M. Scholz [d], J. Svoboda [a,b], J. Swierblewski [d], M. Sos [a,b], M. Tadros [a], P. Titus [e], M. Tomes [a,c], A. Torres [a,h], G. Tracz [d], P. Turjanica [i], M. Varavin [a], V. Veselovsky [a], F. Villone [g], P. Wąchal [d], V. Yanovskiy [a], G. Zadvitskiy [a], J. Zajac [a], A. Zak [a], D. Zaloga [a], J. Zelda [a], H. Zhang [e]

[a] Institute of Plasma Physics of the Czech Academy of Sciences, Prague, Czech Republic
[b] Faculty of Nuclear Sciences and Physical Engineering, Czech Technical University in Prague, Prague, Czech Republic
[c] Faculty of Mathematics and Physics, Charles University, Prague, Czech Republic
[d] Institute of Nuclear Physics Polish Academy of Sciences (IFJ PAN), Kraków, Poland
[e] Princeton Plasma Physics Laboratory, Princeton, NJ, USA
[f] Max-Planck-Institut Für Plasmaphysik, München, Germany
[g] Consorzio CREATE, DIETI, Universita degli Studi di Napoli Federico II, Italy
[h] Instituto de Plasmas e Fusão Nuclear, Instituto Superior Técnico, Universidade de Lisboa, Lisbon, Portugal
[i] Faculty of Electrical Engineering, University of West Bohemia, Pilsen, Czech Republic
[j] Institute of Plasma Physics and Laser Microfusion, 01-497, Warsaw, Poland

ARTICLE INFO

Keywords:
COMPASS-U
High magnetic field
Tokamak design
Thermonuclear fusion

ABSTRACT

COMPASS Upgrade is a new medium size, high magnetic field tokamak ($R = 0.9$ m, $B_t = 5$ T, $I_p = 2$ MA) currently under design in the Czech Republic. It will provide unique capabilities for addressing some of the key challenges in plasma exhaust physics, advanced confinement modes and advanced plasma configurations as well as testing new plasma facing materials and liquid metal divertor concepts.

This paper contains an overview of the preliminary engineering design of the main systems of the COMPASS Upgrade tokamak (vacuum vessel, central solenoid and poloidal field coils, toroidal field coils, support structure, cryostat, cryogenic system, power supply system and machine monitoring and protection system). The description of foreseen auxiliary plasma heating systems and plasma diagnostics is also provided as well as a summary of expected plasma performance and available plasma configurations.

* Corresponding author.
E-mail address: vondracek@ipp.cas.cz (P. Vondracek).

https://doi.org/10.1016/j.fusengdes.2021.112490
Received 27 November 2020; Received in revised form 17 February 2021; Accepted 9 March 2021
Available online 23 March 2021

Table 1
Overview of COMPASS-U engineering parameters.

Quantity		Value
B_t	Toroidal magnetic field	≤ 5 T
I_p	Plasma current	≤ 2 MA
R_{geom}	Major radius	0.9 m
a	Minor radius	0.27 m
A	Aspect ratio	3.3
δ	Triangularity	0.3–0.6
κ	Elongation	≤ 1.8
V	Plasma volume	2.1 m^3
S	Plasma surface at separatrix	13 m^2
T_{vv}	Vacuum vessel operation temperature	≤ 500 °C
P_{NBI}	NBI heating power (initial phase)	4 MW
P_{ECRH}	ECRH heating power (initial phase)	1–2 MW
$t_{flat\text{-}top}$	Flat-top length	2–10 s
Φ_p	Poloidal magnetic flux swing	6.7 Wb

1. Introduction

Next step fusion devices and future fusion power plants based on the tokamak concept are expected to operate at high magnetic field ($B_t \geq 5$ T is expected) and $P_{sep}B_t/(qAR)$ ratio (see Tables 1 and 3 for definition). In contrast to this, present-day tokamaks all over the world can only reach much lower magnetic fields. The existence of such a machine would be an indisputable benefit for fusion research and would allow in-depth studies of many reactor relevant topics.

COMPASS Upgrade (COMPASS-U), a medium-size tokamak (R = 0.894 m, a = 0.27 m), entered the final design phase in the first half of 2020. Delivery of its main systems, machine assembly and commissioning followed by the first plasma is expected in the period 2021−23. COMPASS-U will provide unique capabilities: high magnetic field (B_t = 5 T), plasma current (I_p = 2 MA) and plasma density ($n_e \sim 10^{20}$ m^{-3}) combined with extensive auxiliary plasma heating power: starting with 4 MW of neutral beam injection (NBI) and 1 MW of electron cyclotron resonant heating (ECRH) with foreseen future extensions up to in total 18 MW of combined NBI and ECRH heating power. In addition, the device will be operated with a hot metallic first wall and a vacuum vessel (up to 500 °C).

Due to its capabilities and plasma conditions, the COMPASS-U tokamak will be able to efficiently support physics aspects of the ITER operation as well as to address some of the key challenges for DEMO construction and operation. Namely, it will focus on the divertor physics at DEMO-relevant conditions including plasma exhaust with extreme heat fluxes and advanced confinement modes. In addition, research of advanced materials for Plasma Facing Components (PFC) including liquid metal divertor concepts in later operational phases is envisaged.

Section 2 of this paper presents an overview of the preliminary design of individual tokamak subsystems: an Inconel 625 vacuum vessel and its heating system, a central solenoid (CS) and poloidal field (PF) coils manufactured with a hollow copper conductor, demountable copper toroidal field (TF) coils equipped with bolted and sliding joints, a massive stainless steel support structure, a cryogenic system providing cooling of the support structure and coils down to 80 K, a vacuum cryostat providing thermal insulation of the hot vacuum vessel from the cold coils and support structure, a machine monitoring and protection system, and a power supply system.

Auxiliary plasma heating systems are described in Section 3. Section 4 is devoted to a brief overview of plasma diagnostics planned for COMPASS-U and Section 5 summarizes the anticipated plasma parameters of this new device.

2. Engineering design

The main engineering parameters of COMPASS-U are summarized in

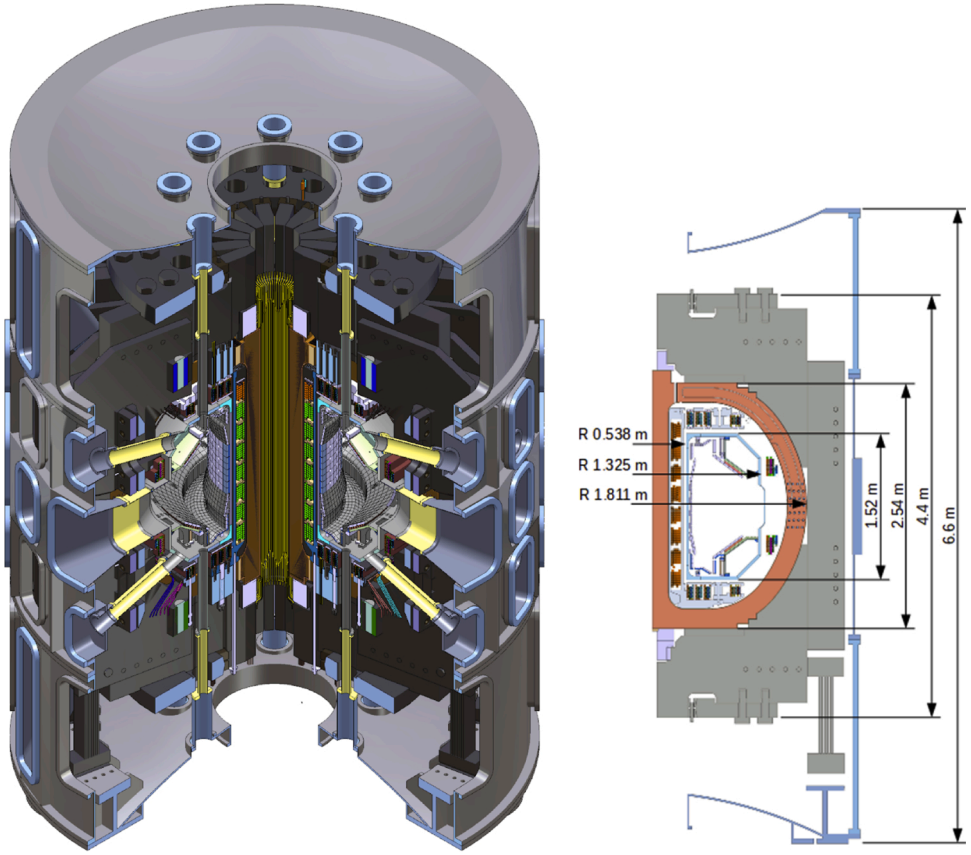

Fig. 1. Cut through the COMPASS-U tokamak.

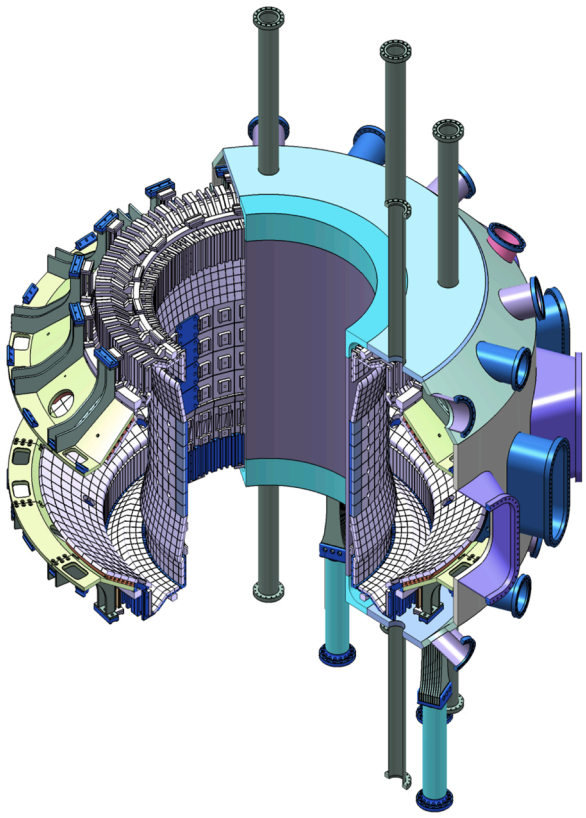

Fig. 2. Cut through the COMPASS-U vacuum vessel, the passive stabilizing plates and the PFCs.

Table 1.

The design of COMPASS-U has undergone significant changes on the way from the conceptual design [1] to the preliminary design of the machine, even though the main parameters have been kept the same. The major differences are reduction of the vacuum vessel wall thickness, movement of the central solenoid inside of the TF volume, enlargement of the TF coils and modification of their joints, significant change in the support structure design allowing vertical disassembly of the machine and modification of the cryostat. An overview of the machine is shown in Fig. 1.

2.1. Vacuum vessel and in-vessel components

The preliminary design of the COMPASS-U vacuum vessel is based on a single wall structure made of Inconel 625. It has a D-shaped cross-section with a 23 mm thick cylindrical inner wall, 35 mm thick flat top and bottom lids and a 30 mm thick outer wall consisting of a cylindrical middle part and upper and lower inclined parts. The vacuum vessel body has an outer diameter of 2.75 m and is 1.52 m high with a total weight of approx. 6 t. A 3D view of the vacuum vessel is shown in Fig. 2.

The vacuum vessel is equipped with 16 equatorial ports of two types: larger funnel-shaped ports (350 mm wide and 500 mm high in the narrowest section) and narrow radial ports (200 mm wide, 500 mm high). There are also 16 lower and 16 upper divertor ports of three different types (DN160 inclined by 0°, 15° and 60° with respect to the horizontal plane) and 8 lower and 8 upper vertical ports (DN100). All port extensions connecting the vacuum vessel and the cryostat have flexible middle sections allowing differential thermal movement of the vacuum vessel. See Fig. 13 for more details.

There are 8 Inconel 625 supports bolted to the lower part of the vacuum vessel connecting it to the lower part of the support structure. The supports are flexible in the radial direction to allow free thermal expansion of the vacuum vessel.

The vacuum vessel size is substantially larger than the plasma size to secure enough space for in-vessel equipment (divertor cryopumps, instrumentation of the future liquid metal divertor, etc.). Passive stabilizing plates (PSPs) are therefore introduced to assure the plasma vertical stability. The passive stabilizing structure consists of two 20 mm thick Glidcop Al-60 (dispersion strengthened copper with high strength at 500 °C) loops in anti-parallel connection through a coaxial bridge. Each stabilizing loop is connected to a 20 mm thick Inconel support structure bolted to pads welded to the vacuum vessel.

The stabilizing effect of the PSPs was assessed using the stability parameter f_s, as defined in [2]. It is the ratio of the stabilizing to the destabilizing force gradient in vertical coordinate. $f_s > 1$ is strictly required for controllable plasma, a requirement of $f_s > 1.5$ for all plasma scenarios was selected in COMPASS-U design. The analysis was performed with FIESTA simulation code [3]. $f_s = 1.85–2.05$ is reached for planned scenarios including the negative triangularity scenario - see Section 5.2 for more details. Possible later removal of the lower PSP is considered as one of options how to accommodate larger high performance plasma with negative triangularity ($f_s \sim 1.7$ in such a case).

Temperature stabilization of the vacuum vessel is secured using a gaseous heating medium (He and CO_2 being the main candidates) running through Inconel heating pipes welded to the inner surface of the vacuum vessel. Foreseen operation temperature of the vacuum vessel is in the range from room temperature to 500 °C.

The outer side of the vacuum vessel is thermally insulated using 20 mm thick thermal multi-layer insulation (MLI) consisting of 30–40 layers of metallic reflectors and glass fibre separators. Electromagnetic forces from disruption-induced currents within the insulation are reduced by using low-conductivity metals (silver coated stainless steel or titanium) as a reflector and having additional insulating cuts in the reflector layers.

An extensive electromagnetic modelling of plasma disruption events expected in the COMPASS-U tokamak was conducted [4,5]. List of disruption sequences which are considered as the most severe for the mechanical design of the vacuum vessel was proposed [4]. All of the critical disruption sequences presume the maximal toroidal field $B_t = 5$ T and pre-disruptive plasma current $I_p = 2$ MA. The following disruption events are represented in the critical disruption sequences: current quench of 3 MA/ms rate, thermal quench (maximal expected plasma energy $W_T = 830$ kJ and quench time $t_{TQ} = 0.1$ ms), slow 35 ms vertical displacement event (VDE) towards passive stabilizing plates, fast 1.55 ms VDE into the divertor region and halo currents bounded by $F \times \mathrm{TPF} = 0.75$, where F is the halo current fraction and TPF is the toroidal peaking factor. Electromagnetic loading resulting from disruptions was used as an input for the subsequent static [6] and transient structural analyses verifying the mechanical design of the vacuum vessel.

COMPASS-U will have metallic PFCs. A large part of the vacuum vessel will be covered by Inconel tiles (possibly with tungsten coating), such as the PSPs, most of the inner (high field side) wall and 8 outer (low field side) wall poloidal rib limiters. High heat flux regions such as the divertor, 8 poloidal guard limiters at the inner wall, and one main outer wall poloidal limiter will be made of bulk tungsten tiles. A lower closed divertor is foreseen for the initial phase of operation. The installation of a second upper closed or open divertor is planned for later operational phases, followed by the installation of a divertor based on liquid metal technology.

All PFCs will be heated and cooled mainly by inter-shot radiation at elevated temperatures. Passive cooling through flexible copper anchors attaching PFC supports to the heating/cooling tubing of the vacuum vessel is considered for low temperature vacuum vessel operation.

2.2. Central solenoid and poloidal field coils

Plasma break-down and ohmic current drive are secured by 8 identical CS segments wound around the central part of the TF coils („TF

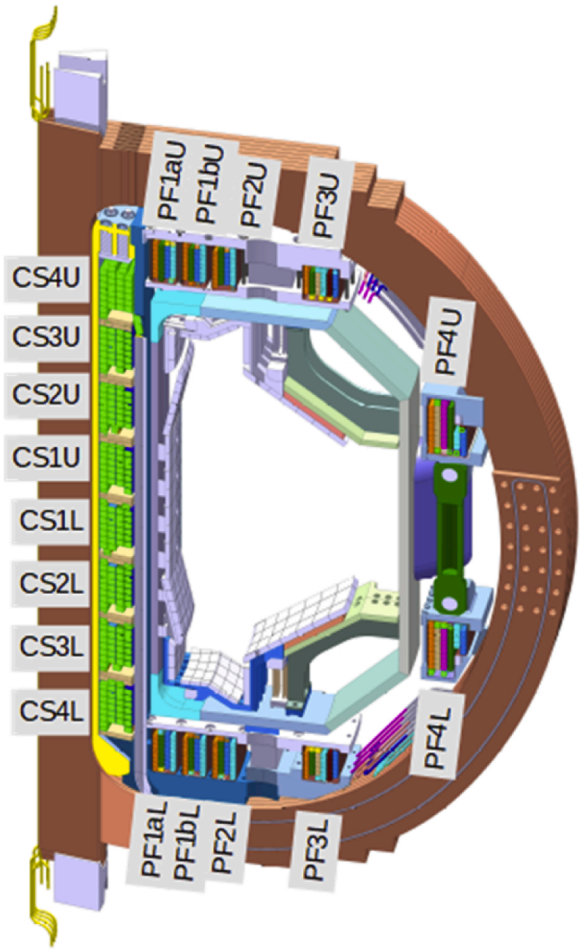

Fig. 3. Poloidal cut through COMPASS-U with labelled CS segments and PF coils.

core"). The CS segments are electrically connected in pairs: CS1U + CS1L, CS2U + CS2L, CS3U + CS4U, CS3L + CS4L (see Fig. 3). Each CS segment has 29 turns of half-hard CuAg0.1 (OF) hollow conductor with outer dimensions 24 × 21 mm and with an elliptical cooling channel. The inner diameter of each CS segment is 0.75 m and the total winding length is ~90 m. Maximum coil current is ±50 kA.

The CS segments are placed inside two tie tubes made of Nitronic 50 alloy and pressed together via a preload mechanism embedded inside the upper part of the inner tie tube. The preload mechanism is based on 80 stacks of heavy duty Belleville washers providing a preload capacity of several MN. The CS assembly is shown in Fig. 4.

COMPASS-U will have 5 upper and 5 lower poloidal field coils in up-down symmetric arrangement (PF1a, PF1b, PF2, PF3 and PF4)–see Fig. 3. The innermost coils PF1a and PF1b are connected in series to a common power supply. PF coil diameters range from 1.2 m to 2.9 m and winding length from 120 m to 360 m. Maximum current of the PF1–PF3 coils is ±25 kA and ±30 kA for the PF4 coil. Similarly to the CS segments, PF coils are wound from a half-hard CuAg0.1(OF) hollow conductor with a circular cooling channel. Conductor dimensions are 15 × 15 mm and 20 × 17 mm for the PF1-PF3 and PF4 coils, respectively. The parameters of the coils are summarized in Table 2.

All the CS, PF and TF coils will be cooled down to ~80 K prior to the plasma discharge to reduce their resistivity by a factor of ~5–7. Gaseous helium flowing through the cooling channels inside the coil conductors will be used as a coolant. The PF coils are divided into several cooling segments to limit the coolant pressure drop to ΔP ~1 bar.

Electrical insulation of the CS and PF coils is achieved by 1 mm thick conductor insulation (kapton tape + S2 glass tape), 0.6 mm additional inter-layer insulation (S2 glass tape, CS coils only) and 3 mm ground insulation (S2 glass tape). The coils will be vacuum pressure impregnated using epoxy resin.

2.3. Toroidal field coils

Up to 5 T toroidal magnetic field (at R = 0.894 m) will be produced by 16 D-shaped coils with 7 turns each (112 turns in total). The coils will be manufactured from 20 mm thick full-hard CuAg0.1 (OF) plates with required yield strength higher than 300 MPa at 80 K. The coils will be insulated by a 1 mm thick layer of E glass which will be vacuum pressure impregnated by epoxy resin. In addition, the coils will have 5 mm thick ground insulation. The overall dimensions of the TF coil assembly are: ~3.6 m diameter, ~2.5 m height and ~24 t weight.

The TF coils have to be dismountable to allow winding of the central solenoid and insertion of the vacuum vessel and PF coils inside the TF volume. The TF coils therefore consist of the central TF core with 16 lower limbs and 16 separate upper limbs. The upper outer limbs are attached to the lower limbs via midplane bolted joints and to the TF core via sliding electrical contacts. The outer bolted joints secure rigid

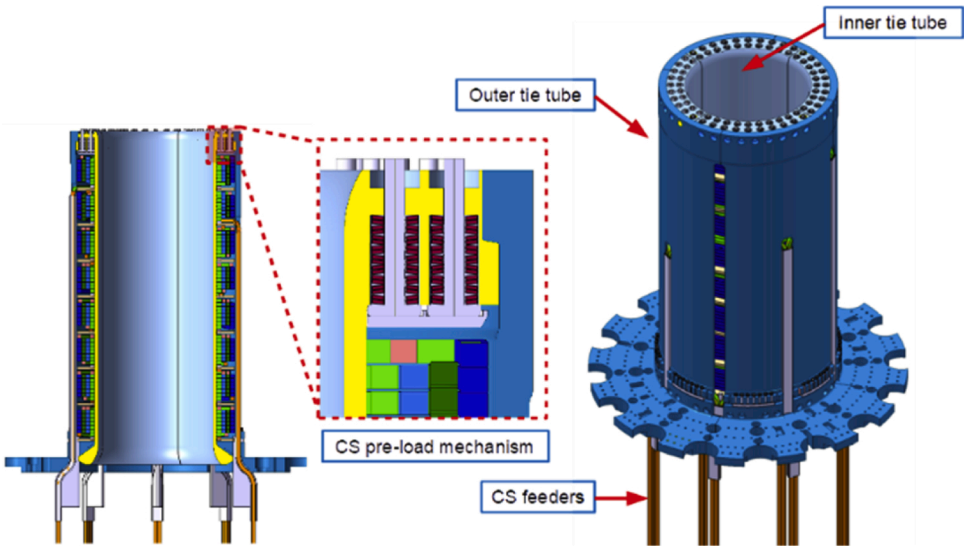

Fig. 4. Vertical cross-section of the CS with a detailed view of the preload mechanism and an overall view of the central solenoid including the tie tubes.

Table 2
Overview of parameters of CS segments and PF coils.

Coil	Current range [kA]	Conductor w × h [mm]	Diameter [m]	Turns	Winding length [m]	cooling segments
8×CS	± 50	24 × 21	0.8	29	90	1
2×PF1a	± 25	15 × 15	1.2	32	120	2
2×PF1b	± 25	15 × 15	1.3	32	137	2
2×PF2	± 25	15 × 15	1.5	32	155	2
2×PF3	± 25	15 × 15	2.1	36	233	3
2×PF4	± 30	17 × 20	2.9	40	360	5

Table 3
An overview of expected COMPASS-U operational parameters.

Quantity		Initial phase		Full heating
		Low current	High current	High current
I_p	Plasma current	0.8 MA	2 MA	2 MA
q_{95}	Safety factor	6.3	2.5	2.5
B_p	Poloidal magnetic field at the outer midplane	0.6 T	1.2 T	1.2 T
P_{sep}/R	Ratio of heating power and major radius	3–5 MW/m	4–7 MW/m	12–16 MW/m
$P_{sep}B_t/R$	Ratio of heating power and major radius multiplied by toroidal magnetic field	14–25 MW T/m	21–32 MW T/m	58–80 MW T/m
$P_{sep}B_t/(qAR)$	Divertor challenge quantifier	0.7–1.2 MW T/m	2.6–3.9 MW T/m	7–9.7 MW T/m
τ_E	Energy confinement time	30–40 ms	60–90 ms	50 ms
n_e	Line averaged electron density	2.1–2.2 × 10^{20} m^{-3}	2.2–2.8 × 10^{20} m^{-3}	2.2–2.8 × 10^{20} m^{-3}
$n_{e,GW}$	Greenwald density limit	3.5 × 10^{20} m^{-3}	8.7 × 10^{20} m^{-3}	8.7 × 10^{20} m^{-3}
T_e	Central electron temperature	2.5–5.5 keV	2.5–4.5 keV	7–8 keV
T_i	Central ion temperature	2.5–5 keV	2.5–4 keV	4–6 keV
β_n	Normalized beta	0.8–1.2	0.8–1.1	1.7–1.8
$n_{e,ped}$	Pedestal top electron density	0.9–1.7 × 10^{20} m^{-}	1.4–2.6 × 10^{20} m^{-3}	1.9–2.4 × 10^{20} m^{-3}
$T_{e,ped}$	Pedestal top electron temperature	0.1–0.5 keV	0.1–0.9 keV	1–1.2 keV
$T_{i,ped}$	Pedestal top ion temperature	0.1–0.5 keV	0.1–0.9 keV	1–1.2 keV
P_{ped}	Pedestal top pressure	13–30 kPa	22–75 kPa	80–90 kPa
v^*_{ped}	Pedestal collisionality	0.4–12	0.1–6	0.12–0.14
ε_{max}	Peak Type I ELM energy fluence	0.3–0.6 MJ/m^2	0.5–1.6 MJ/m^2	1.7–1.9 MJ/m^2
λ_q	Heat flux decay length at the outer midplane	1–2.5 mm	0.5–1 mm	0.5–1 mm

connection of the coils at the outer side and turn-to-turn transition of the TF coils. The inner force-free sliding connection was selected for the inner joint as this would be a highly stressed area in case of rigid connection and the design of such a bolted joint would be very challenging. A TF coils overview and detailed views of the joints are shown in Fig. 5.

The sliding joint design is based on similar concepts used in MAST [7] and Alcator C-mod [8] tokamaks. The sliding surface is provided by four 0.75 mm thick copper felt pads soldered to a flexible finger machined at each upper TF limb turn. Reliable contact with a U-shaped groove machined to each TF core turn is secured by two stainless steel spring plate stacks inserted inside each joint. The spring plate stacks provide ~5 MPa contact pressure at each copper felt pad. Vacuum and low temperature compatible lubricant will be applied to each pad prior to machine assembly.

Cooling of the TF coils down to 80 K is achieved by gaseous helium running through copper tubes soldered into grooves machined in each TF turn. There are 3 separated circuits in each turn: in the TF core, in the lower outer limb and in the upper outer limb. Separate parallel connection of odd and even turns in these 3 segments is foreseen and therefore 6 separated cooling loops will be used. This topology permits the possibility of TF cooling with reduced power even in case of fault of some of the cooling segments.

16 TF coils create an acceptable TF ripple below 0.5 % at the plasma separatrix position without additional ferritic inserts and provide enough space for large vacuum vessel midplane ports and near-tangential injection of neutral heating beams (ripple induced fast ion losses < 3.3 % of NBI power). The current limit of the coils is 200 kA, producing 5 T at the major axis of the machine for 2–3 s flat-top length with 340 MJ energy available from the flywheel generators. The resistance of the TF winding cooled to 80 K is expected to be ~0.8 mΩ.

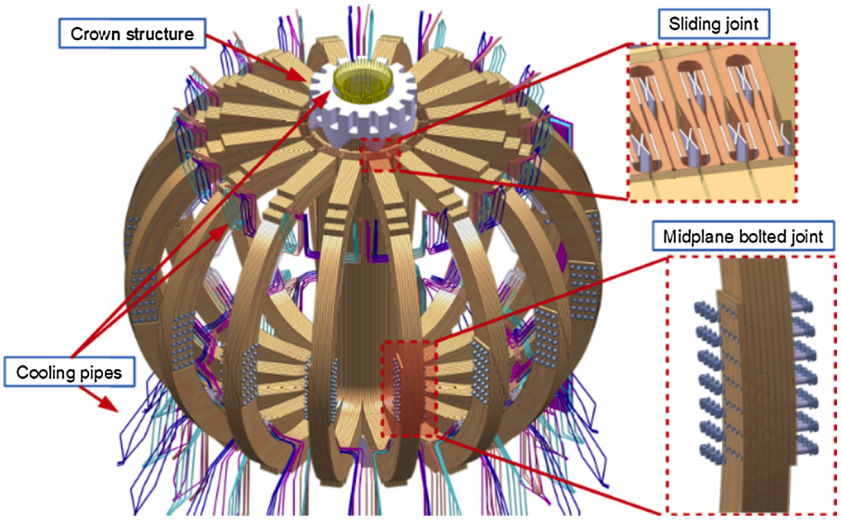

Fig. 5. TF coils with detailed view of the sliding and bolted joint. The CS is not shown in this figure.

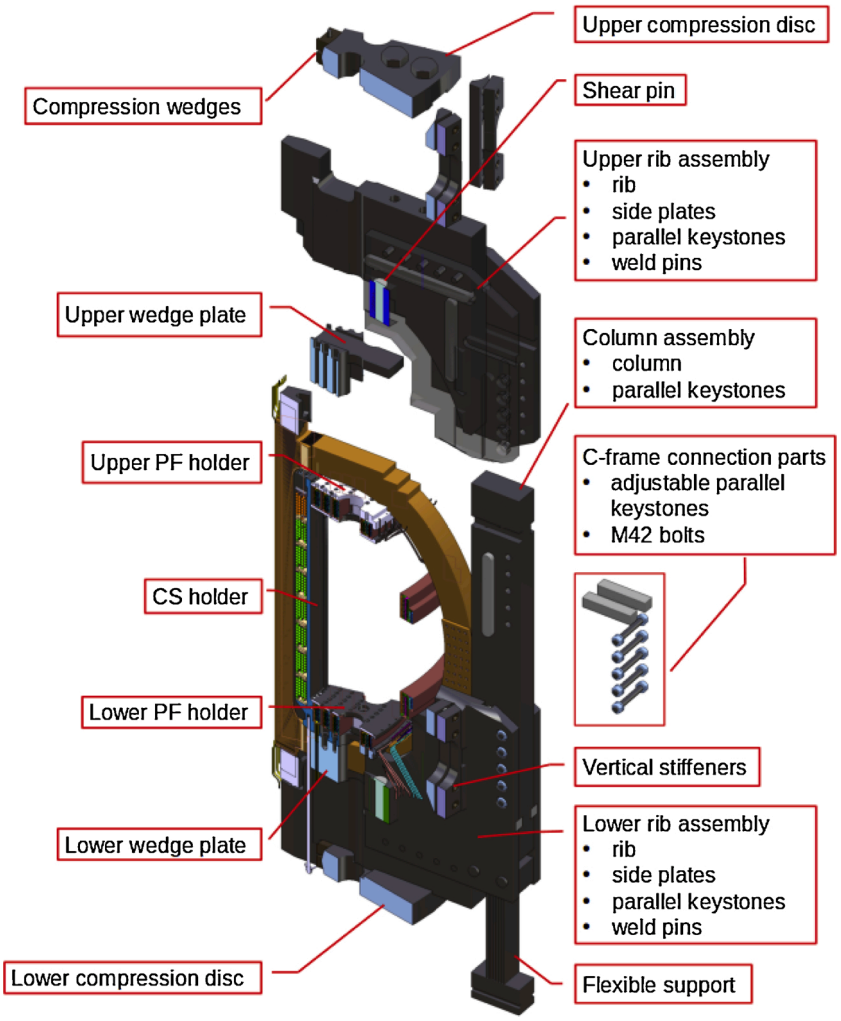

Fig. 6. 1/16 of the COMPASS-U support structure.

2.4. Support structure

The most massive component of COMPASS-U is its support structure, made of stainless steel AISI 304(L)N and 316(L)N. Increased nitrogen content of these steels is important for reaching acceptable strength of the material at cryogenic temperatures (>400 MPa yield strength at 80 K is expected) and to keep the relative magnetic permeability close to 1. The major role of the support structure is to counteract the extreme forces produced by the TF coils (~4–5 MN both in the vertical and radial directions and ~1 MN in the toroidal direction from each TF coil), CS stack (<7 MN vertical force), individual PF coils (<1.5 MN vertical force) and the vacuum vessel during plasma disruption (<4.1 MN vertical, <0.8 MN lateral, <0.2 MN toroidal force). The support structure has to minimize the mutual movement of the TF sliding joints and allow vertical (dis)assembly of the machine. The overall dimensions of the support structure are ~4.5 m diameter, ~4.5 m height and ~190 t weight.

The support structure consists of 16 C-frames, each consisting of a lower rib assembly, a vertical column and an upper rib assembly–see Fig. 6. The three parts of each C-frame are connected via a bolted connection and a set of keystones. All C-frames are held together by 2 large compression disks placed at the bottom and top of the support structure. Torsion of the support structure is reacted by a set of vertical stiffeners placed between the C-frames at the outer side of the support structure. Two massive "wedge plates" create an interface between the C-frames and the TF coils. The CS tie tubes and PF holders are bolted to these wedge plates. The whole structure is supported at the base of the cryostat using 16 flexible supports placed under the C-frames.

Cooling of the support structure is obtained via gaseous helium running through stainless steel pipes welded into machined grooves in the major components of the support structure. Cool-down of the support structure has to be synchronized with the cool-down of the coils to prevent the creation of thermal stresses or gaps in between the support structure and the coils and is expected to take ~1 week.

2.5. Cryogenic system

The COMPASS-U cryogenic system provides cooling of all coils (to increase the electric conductivity) and the support structure (to increase its strength and follow the thermal expansion of the coils). Gaseous helium was selected as the main cooling medium to prevent the danger of thermal shocks and damage of the cooled components by phase changes in the coolant.

Three separate cooling loops are planned:

1) high pressure loop for CS coils cooling, ΔP ~4 bar, mass flow ~80 g/s,
2) medium pressure loop for PF coils cooling, ΔP ~1 bar, mass flow ~160 g/s,
3) low pressure loop for the TF coils and support structure cooling, ΔP ~0.1 bar, mass flow ~800 g/s.

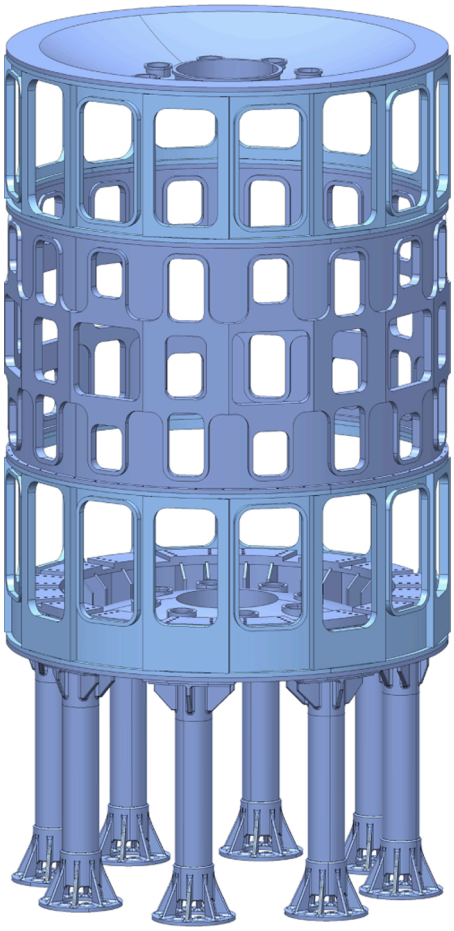

Fig. 7. An overall view of the cryostat resting on 8 columns.

Coolant will be circulated in the cooling loops by turbocirculators. Heat exchange from liquid nitrogen is foreseen as the main "cold source". Future extension by a cycle-based cooler for additional sub-cooling of some cooling loops is possible if needed. The total required cooling power is ~100 kW at 80 K.

The turbocirculators, heat exchanger, control valves, temperature, mass flow and pressure sensors will be located in a vacuum cold-box placed below the tokamak. The cold-box will be connected to the tokamak cryostat via vacuum feedthroughs and a flexible duct to protect the equipment from vibration. The coldox will have its own vacuum pumping system allowing its maintenance without the necessity of breaking the main cryostat vacuum.

2.6. Cryostat

COMPASS-U is enclosed by a cryostat made of stainless steel AISI 304L. It is divided into five major parts: cryostat lower base, lower, middle and upper vertical sections and upper lid. The lower base of the cryostat rests on 8 massive stainless steel columns that are attached to the 800 mm thick steel-reinforced concrete slab of the experimental hall. There are many large service ports in the lower and upper vertical cryostat section allowing good accessibility of the machine during shutdowns without the necessity of lifting the cryostat. The overall dimensions of the cryostat are 4.7 m diameter, 6.6 m height, ~100 m^3 volume. The cryostat is shown in Fig. 7.

The cryostat will be kept at room temperature and will be covered by MLI insulation on the inner surface to reduce the radiative thermal loading of the cryo-cooled components of the machine.

2.7. Machine monitoring and protection

Extreme conditions of operation of individual tokamak systems (temperature ranging from 80 to 800 K, large forces, demanding vacuum conditions, peak magnetic field up to 15 T, cyclic loading, average neutron fluxes ~10^{13} neutrons/cm^2/year) present a major challenge for the machine monitoring and protection system which has to guarantee reliable and safe operation of the machine.

An extensive set of engineering sensors is planned for temperature monitoring: ~800 platinum resistance temperature sensors for monitoring of cold components, >100 type E thermocouples for monitoring of the hot vacuum vessel and optical fibre detectors for monitoring the TF sliding joints in real-time.

More than 300 single axis and rosettes of foil strain gauges in the quarter bridge connection with a dummy strain gauge will be bonded to the coils and support structure to monitor their static and dynamic loading during cool-down and plasma operation. ~30 strain gauges with mineral insulated cables will be spot welded to the vacuum vessel. Movement of the coils and vacuum vessel will be monitored by ~30 displacement sensors.

The resistances of the TF coils and their sliding and bolted joints will be monitored by 3–4 voltage taps placed on each TF turn. Off-line resistance measurement is planned prior to each discharge using several kA current fed to the coils. The resistances of the CS and PF coils will be measured at their feeders and also evaluated from their temperature.

2.8. Power supply system

COMPASS-U will be powered by 4 flywheel generators (GG) with a combined output capability of 263 MW and 490 MJ, connected to the 2 MW public grid available on-site. The 2 existing GGs (2 × 50 MVA, 2 × 50 MJ) will feed the 6 kV grid powering the PF converters, while the 2 new GGs (2 × 102 MVA, 2 × 195 MJ) will feed the 10.4 kV grid powering the TF converters. Junctions between the grids will be implemented for GG redundancy. 38 MW, 58 MJ combined capacity is reserved for the auxiliary plasma heating systems. Schematic overview of the power supply system is shown in Fig. 8.

The PF power supplies will be based on insulated-gate bipolar transistors (IGBT). The whole system consists of 3-phase transformers (2 × 53 MVA) connected to 2 parallel 12-pulse diode rectifiers effectively forming a 24-pulse supply with choke coils for balanced current distribution. These feed a common 950 V DC-link shared by all 12 parallel IGBT H-bridge converters. Water cooled IGBT (with flyback diode modules) at a nominal frequency of 1 kHz will be used. A common capacitor bank of 1 MJ, the IGBT energy dissipator (100 kA/1 s, 250 kA/40 ms), a redundant thyristor crowbar (410 kA) and an output LC filter ($\tau > 5$ μs) will be part of the system. The output parameters of the PF converters are ±25/±30/±50 kA, ±0÷900 V full-load.

The TF power supplies will be thyristor based. The whole system consists of 3-phase transformers (2 × 85 MVA) connected to 2 parallel 12-pulse thyristor converters effectively forming a 24-pulse supply with choke coils for balanced current distribution. All 32 converter blocks will be equipped with fuses at the DC outputs, current commutators for transformer loss of voltage protection and resistive crowbar circuits. The output of the TF converter is 0÷199.5 kA, 0÷780 VDC no-load.

3. Plasma heating systems

3.1. Neutral beam injection

NBI is planned to be the main auxiliary plasma heating system for the initial phase of COMPASS-U operation. Two existing NBIs from the COMPASS tokamak [9] (NBI 1 and NBI 2) with ion energy 40 keV will be upgraded and reinstalled on COMPASS-U to provide up to 2 × 0.5 MW power with pulse length up to ~0.7 s. At least one of these NBIs will be

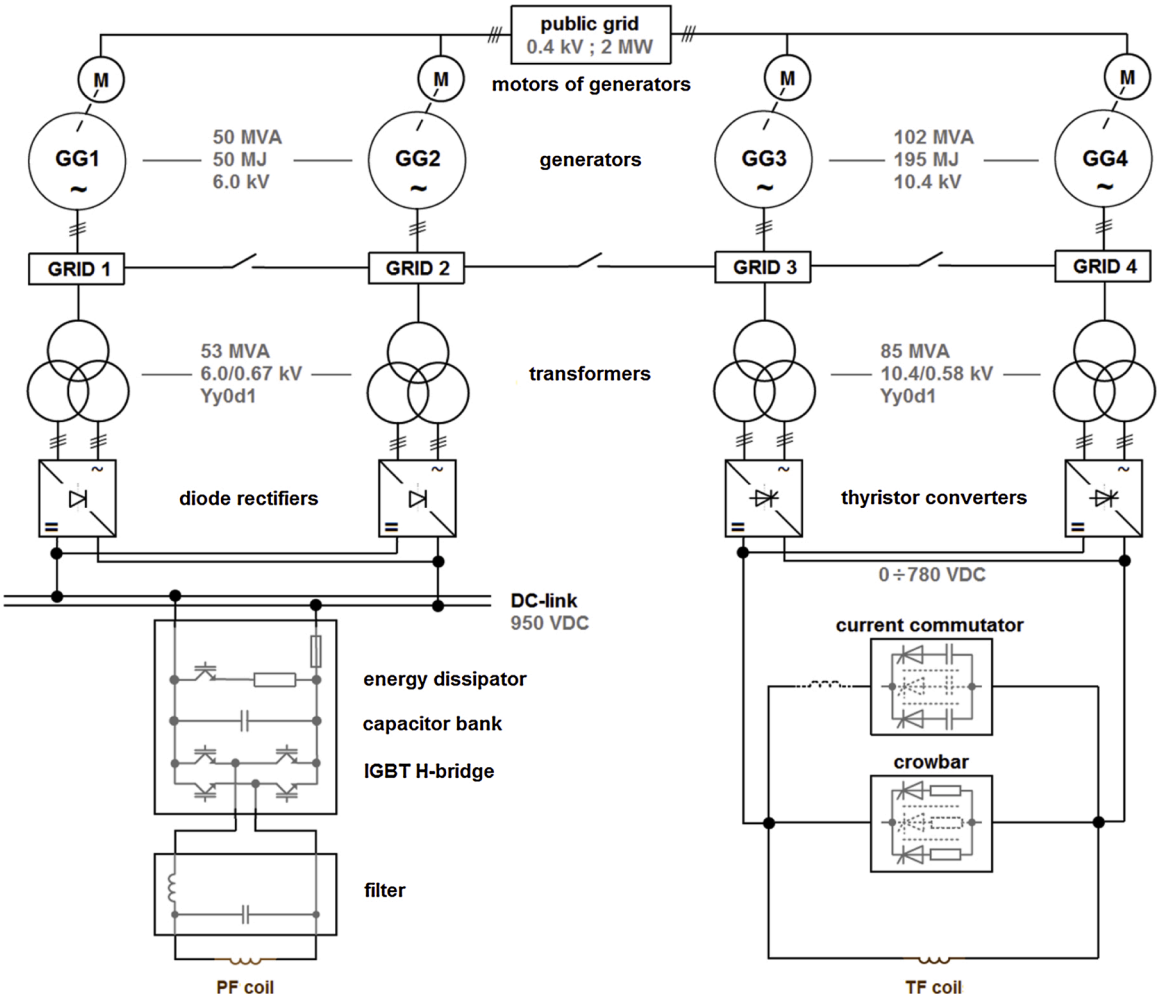

Fig. 8. Schematic overview of the power supply system.

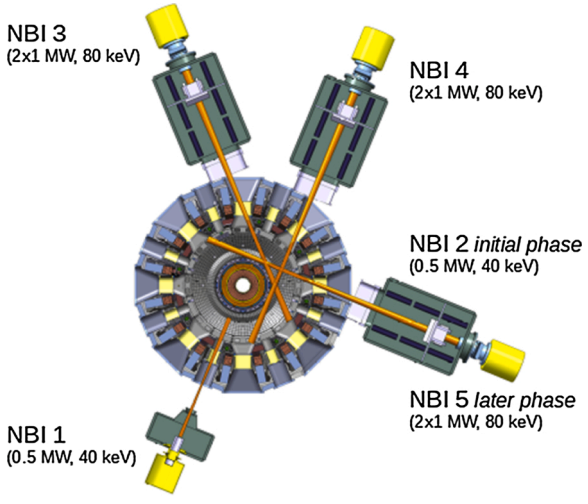

Fig. 9. Midplane cut through COMPASS-U with indicated positioning of NBIs.

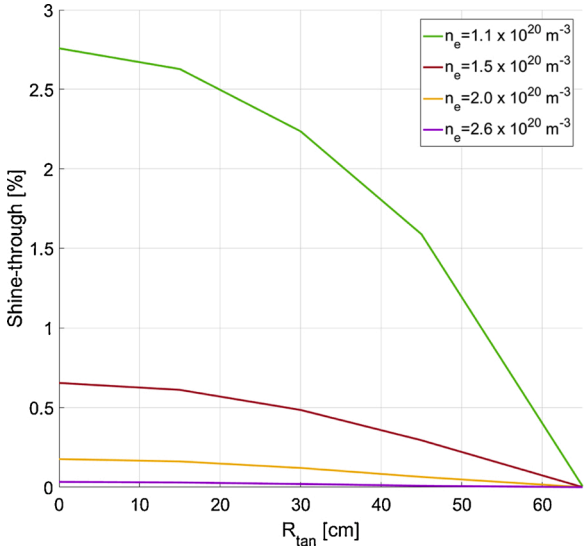

Fig. 10. Fraction (in %) of NBI power lost to shine-through for the various scenarios in COMPASS-U (having different volume average densities), as a function of tangency radius (R_{tan}).

used for diagnostic purposes and positioned in a (near) perpendicular direction.

The new NBIs will be connected to the wide midplane ports in units combining two 1 MW ion sources positioned symmetrically around the machine midplane and inclined vertically by 5–7°. The pulse length of these injectors is ≥1 s. The NBI 3 unit, equipped with one 1 MW ion

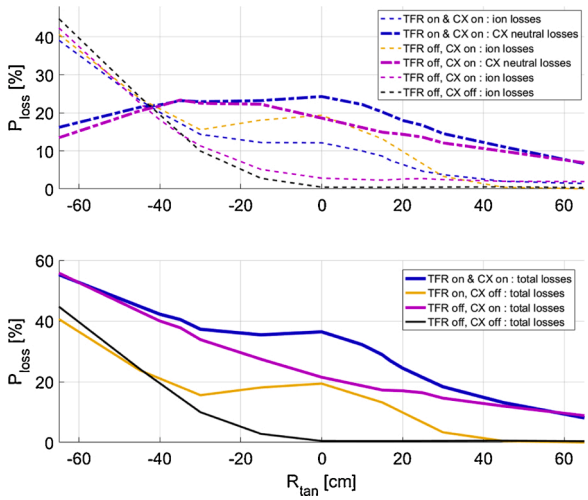

Fig. 11. Fraction (in %) of NBI power lost in scenario 4.4 ($B_t = 4.3$ T, $I_p = 1.4$ MA, $n_e = 1.5 \times 10^{20}$ m^{-3}) of COMPASS-U, as a function of NBI injection tangency radius (R_{tan}). The cases with and without Toroidal Field Ripple (TFR) effects were considered. Regarding the Charge-Exchange (CX) simulated losses, the estimated separatrix neutral density was about 10^{17} m^{-3}.

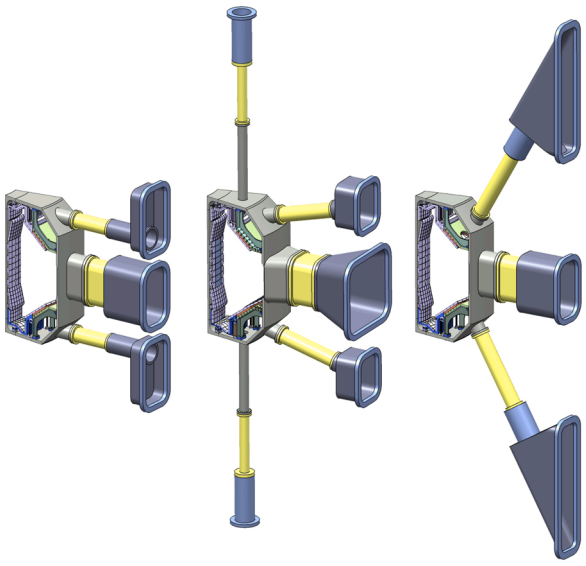

Fig. 13. Three different sections with viewports to the vacuum vessel of COMPASS-U for plasma diagnostics.

source (and prepared for later installation of the second ion source), will be positioned in a co-current configuration for the standard plasma current direction. The NBI 4 unit, equipped with two 1 MW ion sources, will be equipped with a movable stand allowing positioning of the unit in both co- and counter-current directions. The achievable tangency radius (R_{tan}) range will be about -0.6–0.6 m. The installation of another 2–4 MW of NBI heating is planned for later operational phases. An overview of the NBI positioning is shown in Fig. 9.

The NBI power deposition has been shown to be satisfactory within the expected range of density for operation: 1.0–3.0 $\times 10^{20}$ m^{-3}. This is illustrated in Fig. 10. The shine-through remains below 3 % of the injected power in the most unfavourable case (low density, perpendicular injection).

The NBI efficiency in terms of power density deposition has also been studied with the EBdyna code [10] in terms of the percentage of beam lost to the combined effect of the toroidal field ripple (TFR) and charge-exchange (CX) in the edge region. In particular, the NBI has been calculated to be able to achieve low momentum injection using a balanced geometry. This is reflected in Fig. 11. As can be derived from the plot, a reasonable choice in terms of losses for a balanced injection scenario would be a combination of $R_{tan} = -30$ cm and 30 cm. The ratio of injected power should then be lowered for the co-injection beam to compensate for the 38 % of losses in the counter-injection case.

Although the power fraction lost to CX is rather large, it occurs in the edge region of the radial power deposition profile. A simple transport simulation evaluates the associated overall reduction of core temperature to be less than 5 %.

The losses of fast ions and neutrals on the PFCs are expected to remain below 0.2 MW/m^2 in co-injection geometry, well within the acceptable range for the PFCs. However, the induced sputtering of impurities might be a concern and will require monitoring by spectroscopy.

3.2. Electron cyclotron resonant heating

Use of the ECRH system is planned to prevent impurity accumulation

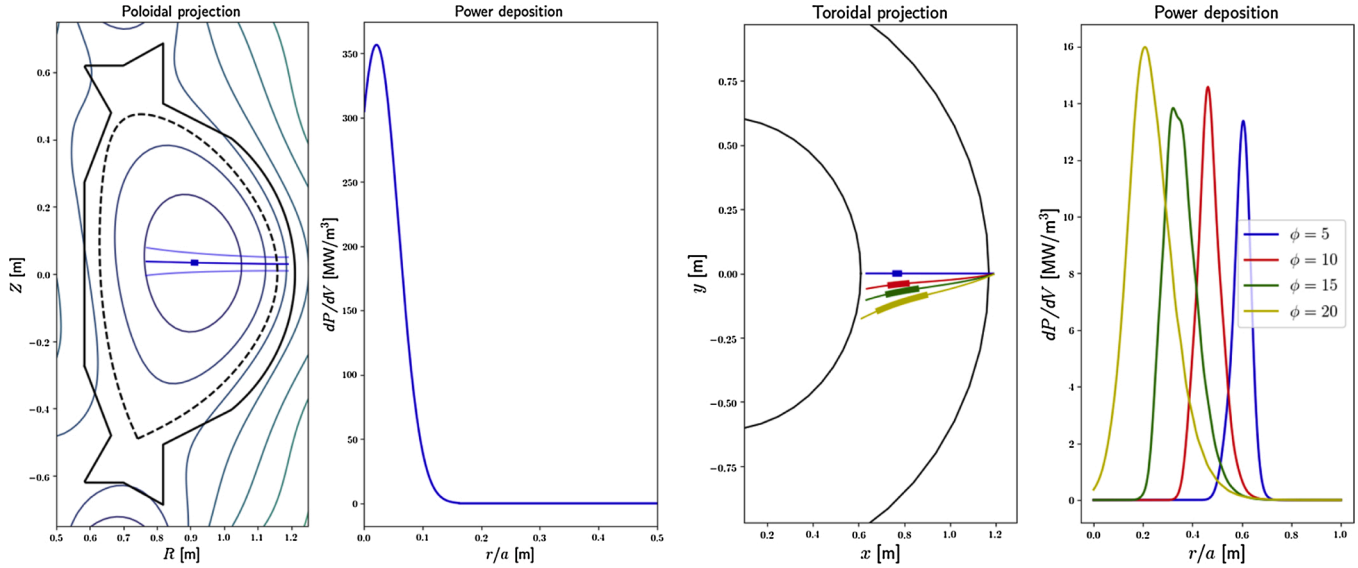

Fig. 12. Examples of 140 GHz ECRH beam trajectory and power deposition profile (left) with direct injection for COMPASS-U scenario 3.4 ($B_t = 2.5$ T, X2-mode) and (right) with toroidal steering for scenario 4.4 ($B_t = 4.3$ T, O1-mode).

in the core, help access H-mode and provide additional heating of the plasma; it will be also used to suppress neoclassical tearing modes and help shaping the plasma profile; and finally, it can be used to assist plasma breakdown, if needed. COMPASS-U is supposed to operate mainly in the range of toroidal magnetic fields between ~2.5 T and 5 T, thus the ECRH must be able to provide efficient central deposition over this range. 105–140 GHz dual-frequency solution was selected as this enables operation in the low and high magnetic field limits. Toroidal steering of the beam will be used in the intermediate magnetic field to move the resonance position towards the plasma centre. Depending on the scenario, different wave polarizations (X-mode or O-mode) and different injection strategies were selected based on calculations with the TORBEAM code [11]. An example of the ECRH absorption profile is shown in Fig. 12. Simulations with the ASTRA code [12] to study the effect of ECRH on transport and plasma performance are ongoing.

The initial available power will be 1–2 MW and this will be increased gradually up to 6–10 MW at full performance. To provide the required power, 1 MW gyrotrons will be used, with some fraction of them capable of dual frequency operation, and with a pulse length up to 5 s. The power will be transmitted from the gyrotrons to the tokamak by evacuated, corrugated waveguides. The cut-off density for 140 GHZ is ~2.4 × 10^{20} m^{-3}, which is ~30 % of the Greenwald density for a 2 MA plasma current.

170 GHz ECRH is considered for some of the gyrotrons planned for the later operational phases as this can provide central energy deposition for scenarios around ~3 T where central deposition of 105–140 GHz is not possible. Such a frequency would also enlarge the operational space in terms of plasma density up to ~3.6 × 10^{20} m^{-3}.

4. Plasma diagnostics

From the first phase of operation, the COMPASS-U tokamak will be equipped with a new set of modern, high-speed and high-resolution diagnostics, ensuring its standard operation and enabling cutting edge research in tokamak physics. This diagnostic set will be extended stepwise, depending on the planned increase of plasma performance via the addition of several MW of auxiliary heating and on the envisaged increase of the vacuum vessel operational temperature up to 500 °C. Developed plasma diagnostics should reflect three main aspects: a) compatibility with unique features of the COMPASS-U device, see the detailed analysis in [13]; b) reliable operation of COMPASS-U in all expected plasma scenarios; c) a physics programme based on divertor operation at high plasma and neutral densities and high heat flux densities.

The presented design of the vacuum vessel, see Section 2.1 for details, allows all the required views for plasma diagnostics, as indicated in Fig. 13. There are 16 toroidal sectors of three different types, each having a tall midplane port (wide-angle or narrow) as well as divertor ports (sloped either horizontally towards the divertor targets; at 15° towards the X-point; or at 60° towards the plasma centre) and every second sector having also a vertical port above and below the plasma centre. The wide-angle diagnostic ports are toroidally paired, facilitating toroidal views through the plasma. However, a near-future plan to operate the tokamak at elevated temperatures above 300 °C represents a major challenge for diagnostic design. Taking into account the tokamak size, it leads to the same temperature range for both the PFCs and the vacuum vessel, which is, moreover, enclosed in the cryostat.

The initial set of diagnostics for COMPASS-U contains a set of magnetic sensors, a microwave interferometer, overview (visible) and interlock (near infrared) cameras, impurity and working gas spectroscopic monitors and hard X-ray and neutron detectors. Other diagnostic tools, which are important for later physics studies, will be added stepwise when available, e.g., high resolution Thomson scattering (core and edge), high-speed infrared and visible light cameras, AXUV diodes and metallic bolometers, soft X-ray detectors, a Zeff diagnostic, core and edge charge exchange recombination spectroscopy, electron cyclotron emission diagnostics, a microwave reflectometer, flush mounted Langmuir and divertor rail probes, reciprocating drives with probe heads and a neutral particle analyser.

The set of magnetic diagnostics will ensure plasma position, shape, current and MHD real-time control. The majority of the magnetic sensors will be located inside the vacuum vessel and, therefore, to ensure high-temperature compatibility, they will consist of metallic and ceramic components only and utilize mineral insulated cables and fibreglass insulated wires. Furthermore, sensors based on a new technology of Thick Printed Copper (TPC) [14] will be used as well for the detection of fast plasma fluctuations. The first such prototypes have been manufactured and passed electromagnetic as well as temperature tests. The main plasma control set of magnetic sensors will consist of Rogowski coils (full and partial) at 4 different toroidal positions, 2 sets of

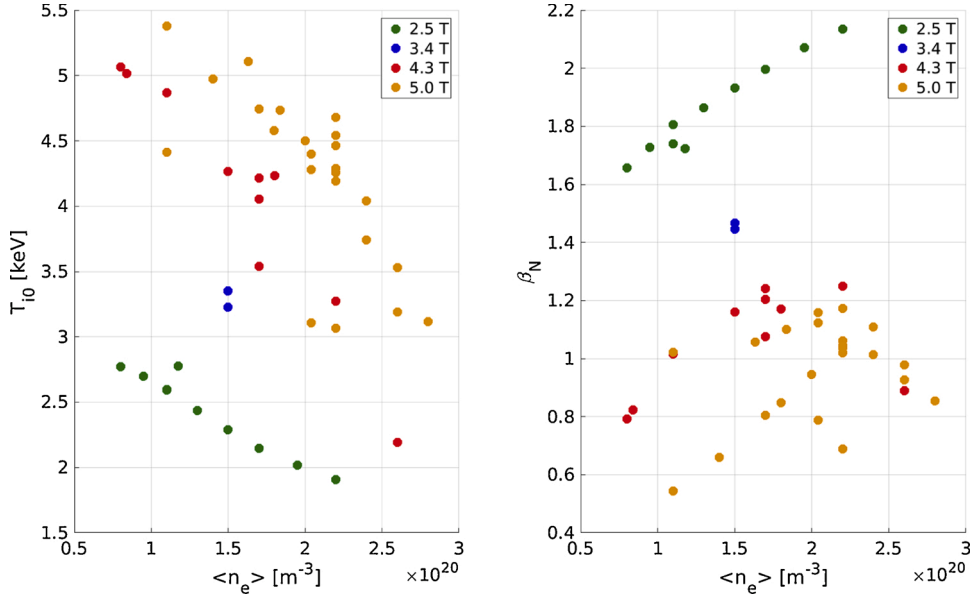

Fig. 14. An overview of the achievable range of core ion temperature and normalized beta during the initial phase of operation (4 MW of NBI heating and 2 MW of ECRH heating were applied).

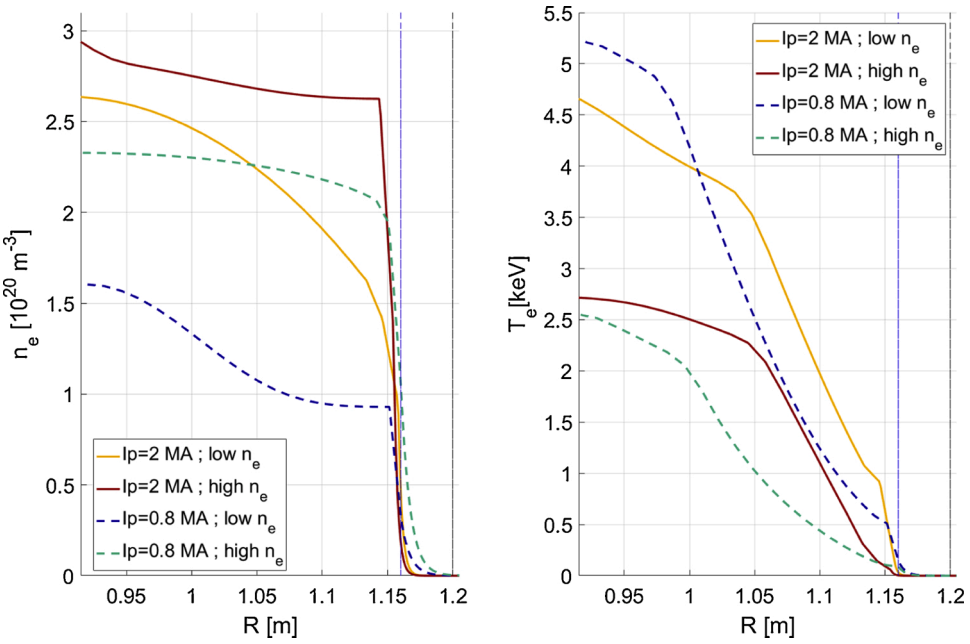

Fig. 15. Typical range of electron density and temperature outer mid-plane profiles expected in COMPASS-U during the initial phase: the low current ($I_p = 0.8$ MA) scenario is in dashed lines and the high current ($I_p = 2$ MA) scenario is in full lines.

23 large-area coils for local magnetic field measurement, 23 pairs (for redundancy) of flux loops, and diamagnetic loops at 5 different toroidal positions. Furthermore, Rogowski coils for measurement of currents in the stabilizing plates and poloidal currents in the VV are included, 3 arrays each of 16 fast, low area coils for fast plasma fluctuations (with one array being the TPC coils), 56 saddle loops and a variety of individual large and small area coils distributed in the toroidal direction to provide toroidal resolution of fast and slow plasma instabilities as well. The ex-vessel diagnostics will consist of 1 full and 1 partial Rogowski coil for VV current measurements and a set of flux loops mounted on every PF coil.

A robust microwave interferometer design, which is resilient to vibrations, was chosen for real-time density feedback. Current technology progress permitted the design of a microwave solution at 400 GHz, providing an unambiguous channel (phase change less than 2π) working well for line-averaged electron densities up to 5×10^{20} m^{-3}. The interferometer antenna system will be oriented horizontally, having a concave reflecting mirror embedded in the PFCs on the central column.

The set of overview and interlock cameras will provide general information about plasma discharge behaviour and possible plasma-wall interaction and will protect the PFCs in real time against local overheating, e.g. caused by fast particles or by the auxiliary plasma heating systems. Their set-up will consist of collection and relay optics, based on a high-temperature compatible first mirror placed near the plasma, and focusing optics, collocated with the camera outside the cryostat.

Basic spectroscopy monitors of the impurities and working gas will be based on two different concepts, which have already been used on the COMPASS tokamak. Fast monitors viewing selected spectral lines will use photomultipliers equipped with appropriate interference filters. Slow monitors will use six compact spectrometers for visible light, near-infrared and near-ultraviolet spectral regions.

Detection of hard X-ray and neutron radiation will be mainly based on scintillators and gas proportional counters. In the early phases of the tokamak operation, their role will mainly consist of monitoring the runaway electron population and providing warnings against potential damage of the PFCs caused by runaways. Monitoring of neutron fluxes (mainly from D + D) will become an increasingly important task following the gradual installation of several MW-class plasma heating NBIs. The aforementioned detectors will either be located at the walls of the experimental hall or shielded in the diagnostic room (spectrometers), where several direct line-of-sight channels towards the tokamak will be provided.

5. Predicted plasma performance

5.1. Plasma parameters

Detailed integrated transport modelling with the METIS code [15] yields density and temperature profiles during the flat-top with 4 MW of NBI heating and 1–2 MW of ECRH heating. We consider a set of equilibria covering magnetic fields and currents ranging from 2.5 T to 5 T and 0.8 MA to 2 MA, respectively. The pressure and current function (RB') radial profiles as obtained from the transport simulations in METIS are used as inputs for the free boundary code FIESTA [3]. Fig. 14 gives an idea of the overall machine performance for a large range of toroidal fields and plasma currents.

The energy confinement time used comes from [16] [ITERH98 P(y, 2)]. Heat diffusivity profile shapes are obtained from a Bohm gyro-Bohm scaling. The ratio of heat transport between electrons and ions is based on the ITG-TEM (Ion Temperature Gradient - Trapped Electron Mode) diagram [17]. The pedestal energy content is obtained according to the difference between the L-mode and H-mode energy confinement time scaling laws [18]

$$P_{\mathrm{ped}} = \frac{1}{3}\frac{1}{V}\left(\tau_{E,H} - \tau_{E,L}\right)\frac{W}{\tau_{E,H}}$$

where V is the plasma volume and W the stored energy in the plasma. Several scenarios are investigated with respect to the foreseen plasma parameters (see Table 3). In the initial phase, 4 MW of NBI heating and 1–2 MW of ECRH will be available. The high current scenario combines the target values of B_T (5 T) and I_P (2 MA), however it requires operation at low Greenwald density fraction (~ 0.3) to maintain efficient heating. At lower plasma current (0.8 MA), higher density fractions (~ 0.6) will become available. Thanks to the large poloidal magnetic field B_p, COMPASS-U will achieve an ITER-relevant range of power decay lengths in the inter-ELM attached H-mode scrape-off layer (SOL), according to the multimachine scaling presented in [19] ($\sim$ 0.5–1 mm). Moreover, the product $P_{\mathrm{sep}}B_t/(qAR)$, often used as a divertor challenge quantifier,

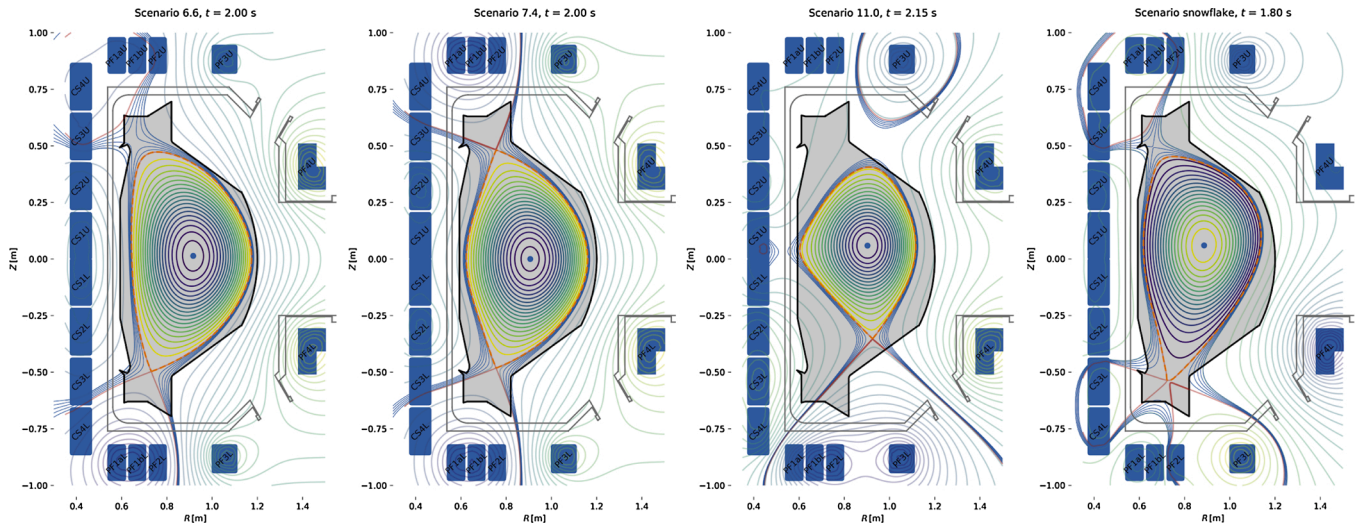

Fig. 16. Examples of COMPASS-U plasma equilibria calculated using the FIESTA code. From left to right: high triangularity single null, medium triangularity double null, negative triangularity single null (I_p = 1 MA), single snowflake (I_p = 1.5 MA).

will reach ITER and DEMO levels (e.g. 9.2 MW T/m is planned for European DEMO [20]) with the foreseen extension of the heating power in later operational phases (14–18 MW). This will make the device an ideal testbed for various power exhaust strategies and divertor concepts.

COMPASS-U will be able to reach very high pedestal pressures especially if Super H-mode access can be realized [21]. High pedestal electron temperatures (see Fig. 15) should provide efficient impurity screening during SOL and divertor region impurity seeding experiments. The collisionality is expressed as

$$\nu^{*}_{\mathrm{ped}} = 6.93 \times 10^{-18} \frac{n_e \Lambda_{ee}}{T_e^2} q_{95} R \left(\frac{R}{a}\right)^{3/2}$$

where density and temperature are measured at the pedestal top and expressed in m^{-3} and eV, respectively, and Λ_{ee} is the Coulomb logarithm for electron-electron collisions. The wide range of pedestal collisionalities will allow for studies of Edge Localized Mode (ELM) properties (as well as ELM mitigation and suppression) for different ELM types [22] and [23].

5.2. Plasma equilibrium

The segmented CS and the set of PF coils close to the plasma column provide a broad range of possible plasma configurations: lower or upper single null and double null configurations with variable plasma triangularity ($\delta \leq 0.6$). Lower, upper or double snowflake and negative triangularity configurations ($\delta \geq -0.3$ within the present location of in-vessel components, $\delta \geq$ -0.5 with modification of the PFCs and PSPs) are achievable for a limited range of plasma current.

Several examples of plasma equilibria reconstructed using the FIESTA code are shown in Fig. 16.

5.3. Neutronics and radiation

The majority of ionizing radiation produced by COMPASS-U will come from beam-target produced neutrons during NBI operation. The

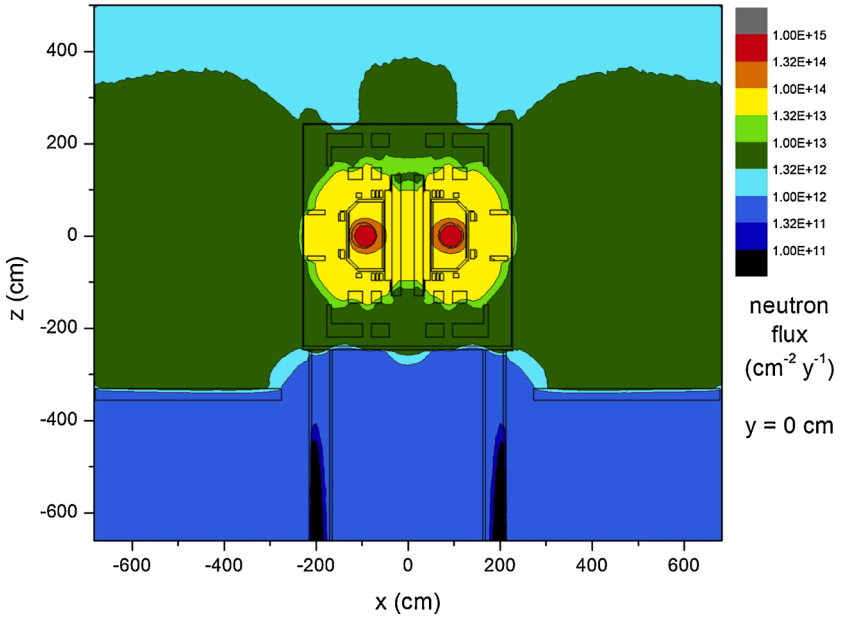

Fig. 17. Vertical cut through COMPASS-U and the experimental hall with a map of neutron flux.

typical expected neutron rate with 4 MW NBI heating ranges from 1×10^{14} neutrons/s to 1.8×10^{15} neutrons/s depending on the plasma scenario. This represents a yearly production of 3×10^{18} neutrons for the expected scenario distribution.

Monte Carlo simulations were carried out with the MCNP code [24] to calculate both the neutron and gamma fields inside the experimental hall. The detailed CAD model of COMPASS-U was elaborated and converted into the MCNP format with the SuperMC program [25]. The obtained spatial distribution of the neutron flux inside the experimental hall is shown in Fig. 17.

An increase of the experimental hall wall thickness to 1.5 m of boron-doped concrete will be provided prior to the assembly of COMPASS-U to provide sufficient radiation shielding.

6. Conclusions

The COMPASS-U tokamak passed successfully its Preliminary Design Review in spring 2020. It aims to become a compact flexible tokamak with parameters relevant to next step fusion devices: high magnetic field, large $P_{sep}B_t/(qAR)$ ratio and high power flux densities in the divertor area, featuring metallic PFCs and operation with a hot first wall.

The preliminary design of COMPASS-U comprises: an Inconel vacuum vessel allowing operation at up to 500 °C; copper TF, CS and PF coils cooled by gaseous helium down to 80 K increasing their conductivity by a factor of 5–7 compared to room temperature; a cooled stainless steel support structure withstanding ~70 MN electromagnetic forces (equivalent to the weight of the Eiffel tower); a power supply system capable of 263 MW of power and 490 MJ of energy. The auxiliary plasma heating is based on a combination of 80 keV NBIs and 105−140 GHz dual frequency ECRH. The overall design provides large flexibility in terms of plasma performance and magnetic configuration.

Declaration of Competing Interest

The authors declare that they have no known competing financial interests or personal relationships that could have appeared to influence the work reported in this paper.

Acknowledgements

This work has been carried out within the framework of the project COMPASS-U: Grants No. CZ.02.1.01/0.0/0.0/16_019/0000768 and LM2018117 are funded by Czech MEYS (Ministry of education, youth and sports.) and co-funded from European structural and investment funds Grant DE-AC02-09CH11466 is funded by US DoE (Department of energy) . The Monte Carlo simulations were performed on the Prometheus cluster at ACC Cyfronet AGH in Cracow, Poland.

References

[1] R. Panek, et al., Conceptual design of the COMPASS Upgrade tokamak, Fusion Eng. Design 123 (2017) 11–16.
[2] J.A. Leuer, Passive vertical stability in the next generation tokamaks, Fusion Technol. 15 (1989) 489–494.
[3] G. Cunningham, High performance plasma vertical position control system for upgraded MAST, Fusion Eng. Des. 88 (2013) 3238–3247.
[4] J. Hromadka et al., Electromagnetic model for finite element analyses of plasma disruption events used in the design phase of the COMPASS-U tokamak, these proceedings.
[5] V. Yanovskiy, et al., Comparison of approaches to the electromagnetic analysis of COMPASS-U vacuum vessel during fast transients, Fusion Eng. Des. 146 (2019) 2338–2342.
[6] N. Patel et al., Design and verification status of COMPASS-U vacuum vessel and stabilization loop, these proceedings.
[7] W. Morris, et al., MAST accomplishments and upgrade for fusion next-steps, Ieee Trans. Plasma Sci. 42 (2014) 402–414.
[8] J. Irby, et al., Alcator C-Mod design, engineering, and disruption research, Fusion Sci. Technol. 51 (2007) 460–475.
[9] R. Panek, et al., Status of the COMPASS tokamak and characterization of the first H-mode, Plasma Phys. Control. Fusion 58 (2015), 014015.
[10] F. Jaulmes et al., Modelling of charge-exchange induced NBI losses in the COMPASS Upgrade tokamak, Submitted to Nuclear Fusion.
[11] E. Poli, A.G. Peeters, G.V. Pereverzev, TORBEAM, a beam tracing code for electron-cyclotron waves in tokamak plasmas, Comput. Phys. Commun. 136 (2001) 90–104.
[12] K.K. Kirov, et al., ECRH power deposition studies in ASDEX Upgrade, Plasma Phys. Control. Fusion 44 (12) (2002) 2583.
[13] V. Weinzettl, et al., Constraints on conceptual design of diagnostics for the high magnetic field COMPASS-U tokamak with hot walls, Fusion Eng. Des. 146 (2019) 1703–1707.
[14] J. Reboun, et al., Properties of power electronic substrates based on thick printed copper technology, Microelectron. Eng. 167 (2017) 58–62.
[15] J.F. Artaud, et al., Metis: a fast integrated tokamak modelling tool for scenario design, Nucl. Fus. 58 (2018), 105001.
[16] ITER, Physics Guidelines, Annex A.1, N 19 FDR 1 01-07-13 R 0.1, 2002.
[17] E. Asp, et al., JETTO simulations of Te/Ti effects on plasma confinement, Plasma Phys, Control. Fusion 47 (2005) 505.
[18] C.F. Maggi, et al., Characteristics of the H-mode pedestal in improved confinement scenarios in ASDEX Upgrade, DIII-D, JET and JT-60U, Nucl. Fus. 47 (2007) 535–551.
[19] T. Eich, et al., Scaling of the tokamak near the scrape-off layer H-mode power width and implications for ITER, Nucl. Fus. 53 (2013), 093031.
[20] G. Federici, et al., DEMO design activity in Europe: progress and updates, Fusion Eng. Des. 136 (2018) 729–741734.
[21] P. Snyder, et al., High fusion performance in super H-mode experiments on alcator C-Mod and DIII-D, Nucl. Fus. 59 (2019), 086017.
[22] A. Loarte, et al., Characteristics of type I ELM energy and particle losses in existing devices and their extrapolation to ITER, Plasma Phys. Control. Fusion 45 (2003) 1549.
[23] A. Loarte, et al., Predicted ELM energy loss and power loading in ITER-FEAT, in: 18th IAEA Fusion Energy Conference (Sorrento, Italy, 2000), IAEA, Vienna, 2001 (ISSN 1562-4153). Can be found at, https://inis.iaea.org/search/search.aspx?orig_q=RN:33029123.
[24] T. Goorley, et al., Initial MCNP6 release overview, Nucl. Technol. 180 (2012) 298–315.
[25] Y. Wu, Multi-functional neutronics calculation methodology and program for nuclear design and radiation safety evaluation, Fusion Sci. Technol. 74 (2018) 321–329.